JGR Earth Surface

RESEARCH ARTICLE
10.1029/2023JF007366

High Basal Melt Rates and High Strain Rates Lead to More Fractured Ice

Ray H. Watkins[1], Jeremy N. Bassis[2], M. D. Thouless[1], and Adrian Luckman[3]

[1]Department of Materials Science and Engineering, University of Michigan, Ann Arbor, MI, USA, [2]Department of Climate and Space Sciences and Engineering, University of Michigan, Ann Arbor, MI, USA, [3]Department of Geography, Swansea University, Swansea, UK

Key Points:

- Basal melt channels and crevasses are key features that affect the topography and roughness of ice shelves
- Roughness is largest in the shear margin where high strain rates and high melt rates increase the formation of channels and crevasses
- We hypothesize that melt rate and strain rate can form weak zones that serve as potential nucleation points for rifting and calving

Supporting Information:

Supporting Information may be found in the online version of this article.

Correspondence to:

R. H. Watkins,
rayhw@umich.edu

Citation:

Watkins, R. H., Bassis, J. N., Thouless, M. D., & Luckman, A. (2024). High basal melt rates and high strain rates lead to more fractured ice. *Journal of Geophysical Research: Earth Surface*, *129*, e2023JF007366. https://doi.org/10.1029/2023JF007366

Received 1 AUG 2023
Accepted 8 APR 2024

Abstract Ice shelves limit the flux of grounded ice into the ocean by buttressing the discharge of land-based ice upstream. Ice shelf weakening and collapse can lead to decreased buttressing and observations increasingly show that some ice shelves have experienced increased melt and increased calving, with recent hypotheses suggesting that increased melt leads to increased fracturing. However, the specific processes that control this correlation are not yet understood, with mechanisms other than melt affecting fracturing. Here we use the topography of the ice shelf base from BedMachine to investigate how basal melting and ice deformation contribute to crevasse and melt channel formation and evolution on the Pine Island Ice Shelf in West Antarctica. We find that high basal melt rates and high first principal strain rates lead to substantial roughening of the ice shelf through a collection of features, including melt channels and crevasses. Critically, melt channels and crevasses are the deepest in all directions at locations where the highest rates of melting and straining occur simultaneously. This suggests that the combination of melt rates and strain rates work in tandem to excavate and seed the deepest melt channels and crevasses on ice shelves. These features then may form lines of weakness that transform into rifts and, ultimately, the detachment boundary for calving events. This implies that melt and fracture play an important role in controlling the dynamics of ice shelves.

Plain Language Summary Future sea level rise is tied to floating Antarctic ice shelves which limit the flow of ice from the continent. Ice shelf collapse could trigger an acceleration of land-based ice into the ocean due to the loss of support, leading to future sea level rise. It has been shown that ice shelves with a higher melt have more crevasses, are more fractured, and are rough. However, the specific processes driving the potential connection between melt and fracture are not well understood. Here we use ice shelf topography to study the relationship between roughness and the size and spacing of geometric features on the Pine Island Ice Shelf. We find that high melt rates and high strain rates result in deeper and wider features on the ice shelf. We also find that, in contrast to the results of previous studies, both melt and fracture contribute to the deepest features. This suggests that these processes contribute to enhancing the depth of features. We hypothesize that this amplifying interaction may then promote rifting and iceberg calving, hinting that it is the combination of melt and fracture that is important in controlling the dynamics of ice shelves.

1. Introduction

Ice shelves are floating slabs of ice that buttress and slow the flow of grounded ice into the ocean (Dupont & Alley, 2005; Gudmundsson, 2013; Haseloff & Sergienko, 2018; O. Sergienko & Haseloff, 2023). Ice shelves are also the primary conduits through which the Antarctic Ice Sheet discharges ice into the ocean. Across all ice shelves, this ice loss takes place roughly equally between basal melting and iceberg calving (Greene et al., 2022; Liu et al., 2015; Rignot et al., 2013). Although not directly responsible for sea level rise, weakening ice shelves and ice shelf collapse can promote the acceleration of grounded ice into the ocean, which does directly contribute to sea level rise (Rignot, 2004; Rignot et al., 2019; Scambos, 2004). Because ice shelves are in contact with both the ocean and atmosphere, ice shelves are thought to be especially susceptible to climate forcing (Obase et al., 2017). For example, the meltwater-triggered explosive disintegration of sections of the Larsen B ice shelf is thought to be related to hydrofractures driven by melt pond formation (Banwell et al., 2013). This breakup, which took place over only 6 weeks in 2002, is linked to atmospheric warming (both long-term and near-term) and highlights the speed at which ice shelves can collapse (Rignot, 2004; Rignot et al., 2019; Robel & Banwell, 2019; Scambos, 2004; Scambos et al., 2003). By contrast, the weakening of ice shelves in the much atmospherically colder Amundsen Sea Embayment, like the Pine Island and Thwaites Ice Shelves, is thought to be linked to ocean

forcing (Jenkins et al., 2018; Lhermitte et al., 2020; Nakayama et al., 2019; Surawy-Stepney et al., 2023; Watkins et al., 2021). Moreover, recent calving events on the Pine Island Ice Shelf have resulted in a significant retreat of the calving front as well as an acceleration of grounded ice upstream of the grounding line (Arndt et al., 2018; Joughin et al., 2021).

Although observations suggest that melting ice shelves are retreating and potentially weakening (Alley et al., 2021; Jeong et al., 2016; Liu et al., 2015), the specific processes linking ice shelf demise to ocean forcing are not yet fully understood. Thinning marine ice and ice mélange, which can stabilize the rifting process (Fürst et al., 2016; Kulessa et al., 2014; Larour et al., 2021), due to climate warming may reactivate dormant rifting. The retreat of ice-shelf calving fronts beyond the "compressive arch" could lead to calving (Doake et al., 1998). Furthermore, the erosion of pinning point contact due to the intrusion of warm waters underneath ice shelves (Still et al., 2018; Wåhlin et al., 2021) can result in a decrease in buttressing and restraining forces that potentially cause crevassing, fracturing, and decreased mechanical stability (Favier et al., 2016; Wild et al., 2022). For instance, the formation of crevasses on ice shelves that eventually penetrate the entire ice thickness and become rifts (Jeong et al., 2016; McGrath et al., 2012) can provide zones of weakness and may seed locations where the ice can fracture and fail.

Melting, in addition to sculpting channels, has been shown to alter existing crevasse penetration depths (Bassis & Ma, 2015; Schmidt et al., 2023) and also promote the nucleation (or excavation) of surface and basal fractures at the apex of basal channels (Alley et al., 2016; Vaughan et al., 2012). As the depth of these crevasses and melt channels approach the ice thickness, the likelihood of calving increases (Bassis & Jacobs, 2013; Bassis & Walker, 2011; Dow et al., 2018). This hints that submarine melting may partially regulate and control crevasse penetration, which itself is related to rifting, iceberg calving, and overall ice shelf dynamics. Critically, all of the processes that impart crevasses and melt channels onto ice shelves may interact and conspire to reduce the mechanical integrity of ice shelves. For instance, melt channels may seed crevasses and crevasses may initiate melt channels. Recently, Watkins et al. (2021) showed that the roughness of ice shelves strongly correlates with basal melt rates. That study hinted that roughness, something easily measurable using remote sensing, might be a proxy for ice shelf structural integrity (Larter, 2022). However, the specific mechanisms controlling roughness, and linking roughness across a range of scales to basal melt, remain unknown. Here we seek to bridge the gap between the complex processes occurring on ice shelves, such as melting and fracturing, and the size of features, such as melt channels and crevasses, to better understand how they interact.

2. Data and Methods

2.1. Study Region

Our study focused on the Pine Island Ice Shelf (Figure 1a) because of the detailed data coverage, which were obtained via Operation IceBridge airborne campaigns, British Antarctic Survey campaigns, and others (Paden et al., 2010; Vaughan et al., 2012). In addition, Pine Island has experienced rapid grounding line retreat (Rignot et al., 2014) and recent large calving events (Arndt et al., 2018; Joughin et al., 2021; Liu et al., 2015). Moreover, a previous study by Watkins et al. (2021) found elevated roughness on the Pine Island Ice Shelf in regions surrounding melt channels, pinning points, shear margins, and rifts. Here we examined two contrasting regions of the Pine Island Ice Shelf in more detail. First, we examined the area surrounding a central flowline in the main trunk of the ice shelf containing documented melt channels (Shean et al., 2019; Vaughan et al., 2012) (blue box Figure 1a). Typically basal melt channels are ∼1–3 km wide and ∼50–400 m deep and occur where a plume of buoyant water melts a trough into the ice-shelf base (Alley et al., 2023).

In addition, we examined the area surrounding a flowline through the shear margin containing crevasses visible in satellite imagery (Lhermitte et al., 2020) and containing melt channels (Alley et al., 2019) (green box in Figure 1a). Most crevasses are taken to be narrow (<500 m), shallow-penetrating fractures (Bishop et al., 2011; Ishalina et al., 2021), however, some have been documented with spacing between 0.5 and 2 km and penetrating hundreds of meters deep (McGrath et al., 2012).

2.2. Ice Shelf Topography

We used gridded inferences of the ice shelf bottom obtained from BedMachine Antarctica Version 2 (Morlighem, 2019), part of NASA's Making Earth System Data Records for Use in Research Environments

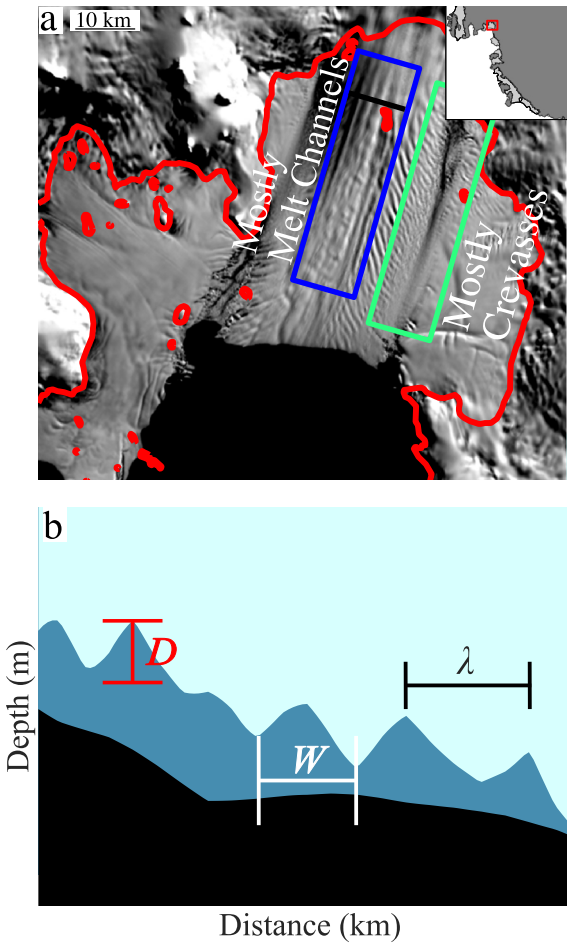

Figure 1. (a) Map of the Pine Island Ice Shelf showing the location of a group of mostly melt channels in the central portion of the ice shelf (blue boxed region) and a group of mostly crevasses in the shear margin of the ice shelf (green boxed region). The black line inside the blue box represents the profile shown in (b). The map inset represents the location of the Pine Island Ice Shelf (red box) within the Amundsen Sea Embayment in West Antarctica. (b) Schematic showing how the depth (D, red), width (W, white), and spacing (λ, black) of features were measured.

(MEaSUREs) program. The products used in constructing the BedMachine ice shelf bottom were collected between 1993 and 2016 (median year of 2012), and the grid posting of the data is 500 m.

Because we used ice shelf base data from BedMachine, ice shelf base data is limited by the hydrostatic assumption and thus, both surface and bottom topography are proportional to ice thickness. Features less than 500 m in width are not resolved by BedMachine and therefore not analyzed in this study. Moreover, the resolution of the data makes it challenging to resolve ice thickness and sub-ice thickness scale features so we do not attempt to correct the hydrostatic assumption to account for flexure. Flexural stresses, like those present around some melt channels, result in patterns of compressive and tensile stresses that enhance local tensile stress fields (Vaughan et al., 2012). However, even when flexural stresses are present, if the larger-scale stress field within the ice is compressive, crevasses are not expected to form (Lai et al., 2020). Although these small-scale features are potentially important in seeding crevasses (Vaughan et al., 2012), our definition of roughness results in a metric that is insensitive to small wavelength features that only make a small contribution to the total roughness. As our focus is on the total roughness and evolution of larger-scale features that are better resolved by the BedMachine data, we opted to focus on the more straightforward method to interpret hydrostatically compensated portion of the topography spectrum.

Generally, for all ice bottom measurements (grounded and floating), errors associated with the BedMachine data products are around 30–40 m but could exceed 250 m in some sparsely surveyed regions (Morlighem et al., 2019). However, when we compare BedMachine data to high-resolution Operation Ice Bridge data (Paden et al., 2010), we find that the mean absolute error of BedMahcine ice base measurements on the Pine Island Ice Shelf is approximately 30 m (Figure S1 in Supporting Information S1). This is likely an appropriate estimate of the ice base error of Pine Island as the ice shelf is densely sampled in the BedMachine model (Morlighem et al., 2019). However, the true error in the data from BedMahcine could be higher or lower: First, features are likely to have advected and (may have) evolved in the 10 years between the collection of these data sets which could lead to overestimating the uncertainty. Likewise, while dense, there are still sections of Pine Island that are under surveyed which could result in an underestimation of the uncertainty. Additionally, for some of the other ice shelves examined later in this study, track distribution is less dense (but more so than other portions of the ice sheet), and errors in ice thickness (and therefore roughness) could be higher. To examine this further, we performed an error analysis based on wavelength and found that error increases as a function of wavelength (Figure S2 in Supporting Information S1). As we are generally concerned with features less than 3 km in wavelength, this result also hints that although the error in sparsely data-covered regions could be quite high the error may be significantly smaller in the other ice shelves in our study that have fewer field collected data points that Pine Island. Finally, we further compared features visible in the BedMachine data with features visible in satellite imagery in our survey regions and found excellent agreement indicating that the features we examine are robust and not artifacts of sparse data combined with the BedMachine inversion process.

2.3. Flow Lines Through the Main Trunk and Shear Margin of Pine Island Ice Shelf

We traced two flowlines from the grounding line to near the calving front of the Pine Island Ice Shelf using velocities from NASA's MEaSUREs data set (Rignot et al., 2013). The flowlines were chosen to pass through the main trunk of the ice shelf, aligning with a basal melt channel (Vaughan et al., 2012) (central flow line, blue box of Figure 1a), or the shear margin of the ice shelf, containing mostly crevasses (shear margin flow line, green box of Figure 1a). These flow lines extended to near the calving front, which has retreated since the satellite composite

images shown were taken. We also traced a sequence of transects perpendicular to the flow lines to sample both longitudinal and transverse to flow portions of basal melt channels and crevasses. Each transect is spaced approximately 500 m apart on the flow line and metrics (depth/width) are measured as an average across the transect.

2.4. Strain Rates and Melt Rates

Strain rates were calculated from surface velocity data derived using feature tracking between pairs of Sentinel-1 Synthetic Aperture Radar (SAR) images. Between October and December 2014, at the start of the EU Copernicus Program Sentinel-1 mission, 9 sequential images were acquired, enabling feature tracking between 8 image pairs separated by 12 days. Standard Gamma Software procedures were used (e.g., Luckman et al., 2015), feature tracking window sizes were 416 × 128 pixels (~1 km in ground coordinates) and displacements were sampled every 50 × 10 pixels (~100 m in the ground distance). The resulting displacement fields were converted to velocity (divided by 12 to give meters per day), filtered using the signal-to-noise ratio, and geocoded to the standard polar stereographic coordinate system at a grid resolution of 100 m. The eight velocity maps were averaged to produce a smoother 2014 product. The magnitude of the first principal strain rate was calculated in a 3 by 3 neighborhood from this projected velocity field. In addition, we used first principal strain rate data obtained from Alley et al. (2018) to perform a continent-wide analysis. We used gridded melt rate products obtained from Adusumilli et al. (2020), which used data between 2010 and 2018 and is posted at a grid resolution of 500 m. Where applicable, the melt rate and strain rate data are interpolated from the gridded products along the flow line.

2.5. Depth, Width and Spacing of Features

We defined "features" broadly as any topographic depression in the base of the ice shelf with a width comparable to or greater than the ice thickness. This includes melt channels and crevasses that are greater than 500 m in width. As we cannot resolve features smaller than 500 m due to data limitations, they are not considered in this study. We then characterized these features using the depth, width, and, when applicable, spacing between features (illustrated in Figure 1b). We defined the depth (D) of a feature as the average of the vertical distance between the two local minima (lowest local point along the transect in the data) at our spatial resolution (or in the case of channels, the deepest flanks) and the local maximum (or in the case of channels, the apex) of a feature on the ice bottom (red line in Figure 1b). The width of a feature (W) was defined as the horizontal distance between two local minima in the ice bottom along a transect (white line in Figure 1b). This width represents the apparent "width" of the feature transverse to the flowline. We also defined the spacing between features (or wavelength) (λ) as the horizontal distance between two local maximums in the ice bottom (black line in Figure 1b). This is taken as the distance between features from left to right in the transverse direction.

2.6. Roughness

Roughness is defined here as topographic variations in the ice base varying from crevasses to large melt channels and rifts. As in Watkins et al. (2021), we followed Whitehouse (2004) and quantitatively defined roughness in a given direction (units meters) using the square root of the integral of the power spectral density $S(k)$ (units m^3):

$$R_{Dir} = \sqrt{\int_{k_1}^{k_2} S(k)dk}. \quad (1)$$

Here, $S(k)$ is the power spectral density of the ice shelf base, which is obtained using a continuous wavelet transform (Sifuzzaman, 2009; Watkins et al., 2021). The power spectral density is a measure of how much power (or magnitude) a given profile has as a function of wavelength (or wavenumber) (Stoica & Moses, 2005). In addition, k (1/m) represents the wavenumber, defined as the inverse of the wavelength. The values $k_1 = 10^{-4}$ (1/m), $k_2 = 2 \times 10^{-3}$ (1/m) represent the bounds of integration in wavenumber space that define the portion of the spectrum over which roughness is calculated. These bounds correspond to wavelengths between ~500 m and ~10 km, chosen as they represent the data resolution and approximate maximum feature size respectively. We also defined the along-flow (R_x) and transverse-to-flow (R_y) roughness for each point on the flowlines. The roughness at a given point is then defined as:

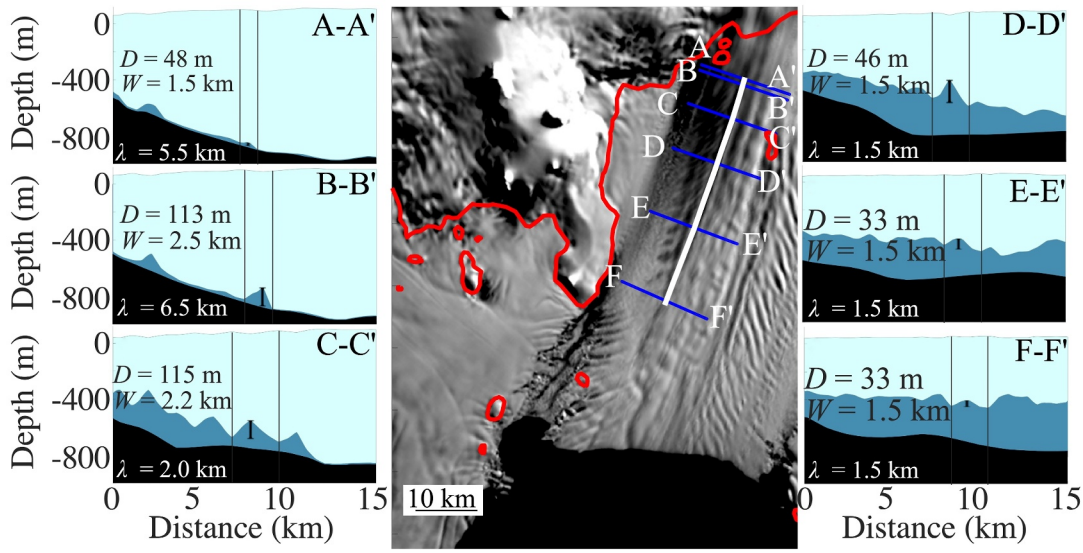

Figure 2. Feature growth and decay on the Pine Island Ice Shelf. Panels (a–c) show the initial growth in width and depth and decrease in spacing as channels advected downstream of the grounding line. Panels (d–f) show the later decrease in depth of the channels with near-constant width and spacing further down the profile. The red line on the map indicates the grounding line. The black vertical lines in each panel show how a single feature evolves across panels. Note that this part of the transect is floating, as is shown in Figure 3a. The white line represents the flow line analyzed. Reported values represent averages across the transect.

$$R = \sqrt{R_x^2 + R_y^2}. \tag{2}$$

This definition of roughness includes topographic variation both normal to and orthogonal to the flowline. We did a sensitivity study where we calculated roughness along different orthogonal directions and found that the total roughness, defined by Equation 2, was insensitive to the orientation of the axes. In addition, by defining roughness in this way, we can generate a 2D gridded roughness map of the entire ice shelf (Figure S3 in Supporting Information S1).

3. Results

3.1. Central Flow Line

We first examined a region on the Pine Island Ice Shelf where a series of melt channels that are aligned mostly in the along flow direction have been identified (Shean et al., 2019; Vaughan et al., 2012). We tracked the depth, width, and spacing of channels using a sequence of transects, both along and transverse to the flow line. The transects, which are depicted by the various panels in Figure 2, started from their origin near the grounding line. These transects along the flow line approached the calving front, where we could no longer identify undulations in basal elevation.

3.1.1. Channels Grow Rapidly, Then Decay

From Figures 2a and 2b, we see the central channel that initiated near the grounding line deepened and widened rapidly, more than doubling in depth from ~48 to ~113 m and widening by ~1 km (1.5–2.5 km). These increases happened after only 1 km of ice flow, with channel spacing remaining roughly 6 km. As additional channels formed between the initial ones, the channel spacing decreased to ~2 km (Figure 2c). The channels reached both their maximum depth (~115 m) and maximum width (~2.5 km) about 15 km downstream from the grounding line (Figure 2c). The width and depth of channels then decreased (Figures 2c and 2d), but the channel spacing remained roughly constant at ~1.5 km. Further downstream, the channel depth decreased until we could no longer identify the channels in the ice shelf bottom (after Figure 2f), which occurred within 10 km of the calving front.

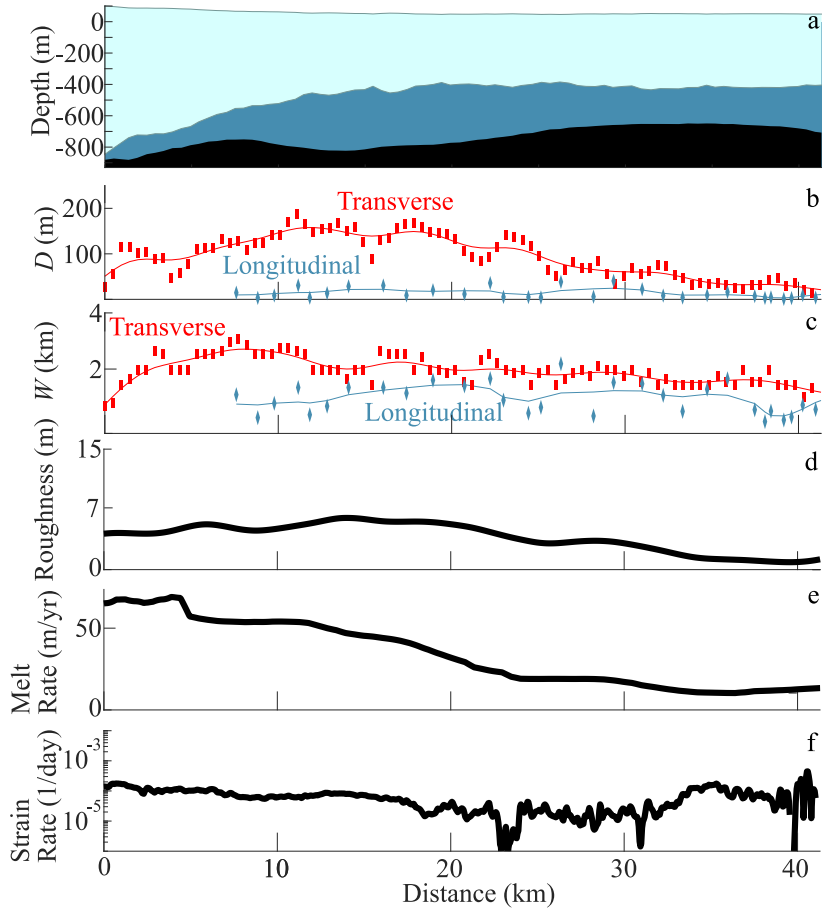

Figure 3. (a) The along-flow profile of the flow line (white line) is shown in Figure 2, which extends from the grounding line to near the calving front. (b) The transverse (red) and longitudinal (blue) depth of features on the ice shelf. The solid lines represent a moving mean of the data points. (c) The transverse (red) and longitudinal (blue) width of features on the ice shelf. Solid lines represent a moving mean of the discrete measurements. (d) The roughness of all features along the flow line on the ice shelf. (e) The melt rate along the flow line. (f) The first principal strain rate along the flow line.

By contrast, we see little change to the width or depth of features in the longitudinal-to-flow profile from the grounding line to near the calving front (Figures 3a–3c). We found that as expected, on average, the features in the transverse-to-flow profiles (blue lines in Figure 2) were deeper (~83 m) and wider (~2.0 km) than their longitudinal-to-flow (white line in Figure 2) counterparts (~14 m depth and ~1 km wide). We also computed roughness (Figure 3d) and because the depth of features was much smaller longitudinal-to-flow than in the transverse-to-flow direction (Figure 3b), roughness (which includes both directions) followed a similar trend to transverse-to-flow depth (Figure 3d).

3.1.2. Comparison Between Central Flow Line Features (Channels), Melt Rates, and Strain Rates

To better understand what drives channel growth and decay, we next compared the melt rate and largest principal strain rate to the depth, width, and roughness derived along the channel (Figures 3e and 3f). The melt rate along the channel was variable, ranging from over 50 m/yr to nearly ~0 m/yr, with much of the high melt occurring within the first 25 km of ice flow. This corresponded with the widening and deepening of all channels. The channels then started to decrease in depth as the melt rate fell below ~25 m/yr. This closure is likely related to a combination of creep closure and differential melting. Additionally, no melting/freeze-on in the channel and high melting on the channel flanks (Dutrieux et al., 2013; Humbert et al., 2022) would also cause channel size decrease.

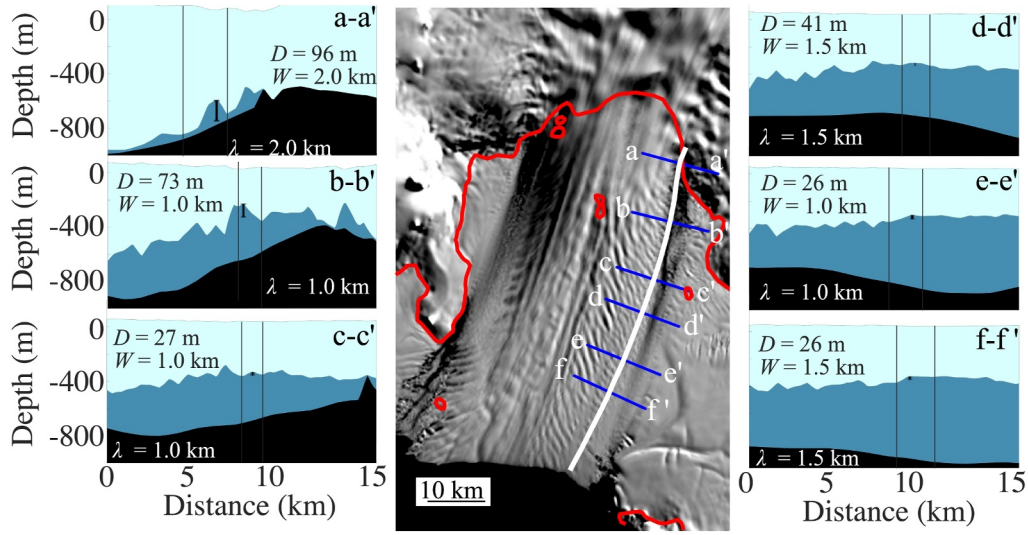

Figure 4. Feature growth and decay in the shear margin of the Pine Island Ice Shelf. Panels (a and b) show the growth in the number of features depicted, which led to a slight decrease in depth and larger decreases in width and spacing. Panels (c–f) show a shrinking of the features which resulted in a decrease in depth and little change in width and spacing. The red line on the map indicates the grounding line. The black vertical lines in each panel show how a single feature evolves between panels. The white line represents the flow line analyzed. Reported values represent averages across the transect. Note that the transects shown here are different than the transects shown in Figure 2.

In contrast, the strain rate along the channel was nearly constant, with a mean value of 1×10^{-4} 1/day, not exceeding 2×10^{-4} 1/day and rarely dropping below 0.5×10^{-5} 1/day. We also examined the smallest principal strain rates and found they aligned roughly transverse to the channel and were, on average, smaller and negative (approximately -1×10^{-5} 1/day). This indicates that the channel closing is due to the (small) compressive strain rates. This secondary flow acting to close the channel is what we expect based on modeling studies (Bassis & Ma, 2015; Drews, 2015).

3.2. Shear Margin Flow Line

To contrast with the central flow line, we also examined profiles along the shear margin of the Pine Island Ice Shelf where heavily crevassed sections of the ice shelf are prevalent (Figures 1a, 4, and 5). We again tracked the width, depth, and spacing of features in the shear margin using transects both along and transverse to the flow line. The transects are once again depicted by various panels (Figure 4) and started from their origin near the grounding line and then ran to near (roughly 10 km, about the size of an iceberg), the calving front, where we could no longer identify the features in the margin flowline.

3.2.1. Features in the Margin Deepen Then Decay

Examining a series of transverse-to-flow features (Figure 4) we found that transverse features, similar to channels, formed as soon as the ice became buoyant at the grounding line. Between their initiation (Figure 4a) and the halfway point of the flow line (Figure 4c), the features reached a maximum depth of ~160 m and a maximum width of ~2.0 km. After this point, the features appeared to be in quasi-steady state, with nearly constant width and depth (mean width of 1.5 km and mean depth of 26 m). The transverse-to-flow features had a characteristic spacing of ~1.5 km between features. This pattern of evolution generally mimicked what we found for the transverse profiles of the central flow line (melt channels).

Like the central flow line, features in the shear margin were on average wider in the transverse-to-flow direction (~2 km, Figure 3c) than the along flow direction (~1 km, Figure 3c). In the shear margin the mean feature depth in both the longitudinal and transverse to flow directions was ~46 m and ~67 m, respectively. The values in the longitudinal direction are larger than those observed along the central flow line, suggesting that features cut across the flow line at an angle, rather than being aligned with the flow direction. Elevated feature depth in both

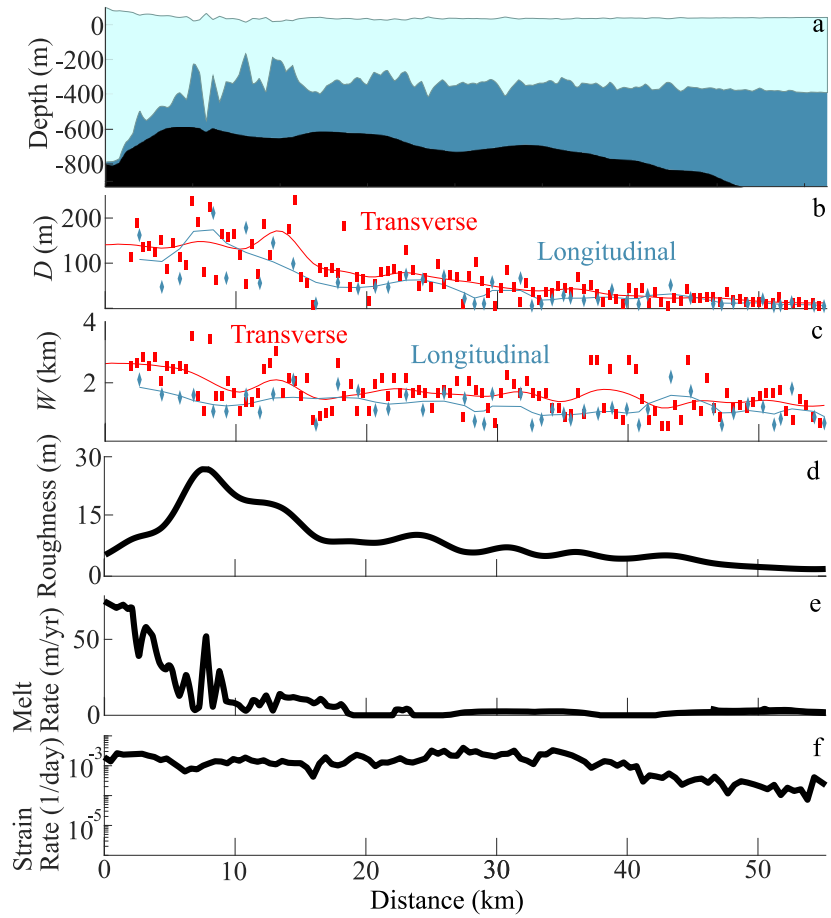

Figure 5. (a) The along flow profile of the shear margin flow line extending from the grounding line to near the calving front (white line shown in Figure 4). (b) The transverse (red) and longitudinal (blue) depth of features on the ice shelf. Here, the solid lines are a moving mean and the data points are the discrete measurements. (c) The transverse (red) and longitudinal (blue) width of features on the ice shelf. Again, the solid lines are a moving mean and the data points are the discrete measurements. (d) The roughness of all features along the flow line on the ice shelf. (e) The melt rate along the flow line. (f) The first principal strain rate along the flow line.

directions results in a roughness nearly double that of the central flow line (11 vs. 6 m), showing that rougher features are tied to deeper features (in both directions). As before, as the ice flowed toward the calving front, the feature depth and the roughness decreased. We also found that the width of the features in the transverse direction decreased from ~3.5 to ~1 km along the profile, while the width of the same features in the longitudinal direction was nearly constant at ~1.0 km.

3.2.2. Comparison Between Shear Margin Features, Melt Rates, and Strain Rates

Similar to the central flowline, we compared the width and depth of features to melt rates and strain rates. Melt rates are highest near the grounding line (~65 m/yr), but fell off rapidly downstream to nearly 0 m/yr (Figure 5e). Over this interval, shear margin features (crevasses and channels) continued to deepen both transverse-to-flow and longitudinal-to-flow. By contrast to the central flowline, the strain rate is over an order of magnitude higher (1.3×10^{-3} vs. 1×10^{-4} 1/day). This strain rate varied along the profile, ranging over two orders of magnitude from 4×10^{-3} to 5×10^{-5} 1/day (Figure 5f). The elevated strain rate corresponded with a significant growth of features in both directions and this growth seems to be especially pronounced in regions that also experienced high melt rates.

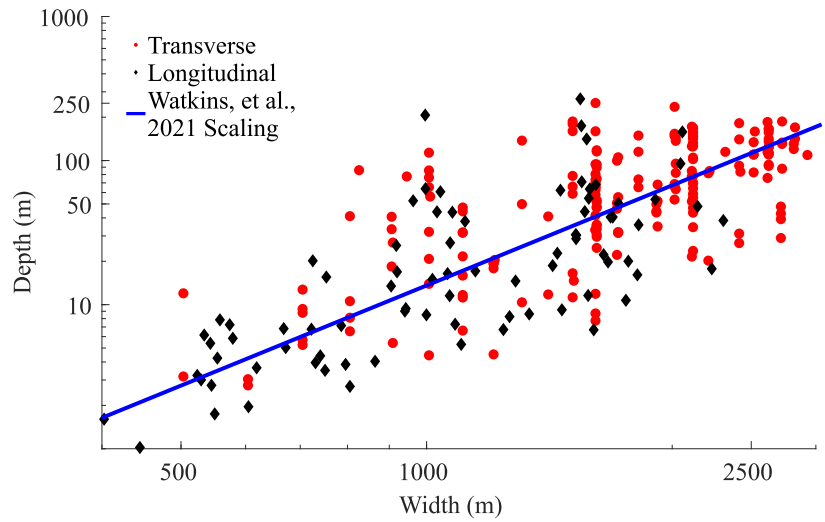

Figure 6. Width versus Depth of all features considered in this study. The black diamonds represent longitudinal features, while the red dots represent transverse features. Note that the scaling here (data points, slope ≈ 2.2) is nearly the same as in Watkins et al. (2021) (blue line, slope ≈ 2.3), in which the scaling follows a power law.

4. Discussion

4.1. Comparison Between Features in the Central Flow Line and Shear Margin Flow Line

Our results support evolution patterns for basal melt channels consistent with previous studies where channels initiate near the grounding line, deepen downstream in the presence of large basal melt rates, and then begin to close as they advect to regions with lower melt rates (Alley et al., 2016; Marsh et al., 2016). Our analysis of the BedMachine product showed that basal melt channels on the Pine Island Ice Shelf typically have widths that range between 1 and 3 km, consistent with previous studies (Vaughan et al., 2012). We also determined a characteristic spacing between channels that varied between 2 and 6 km near the grounding line, with the range narrowing to 1–2 km once the channels were fully formed downstream. The decrease in width is a result of the appearance of channels between the initial channels. This spacing is also similar to the range of spacing estimated based on a linear stability analysis of channel formation (Dallaston et al., 2015).

We find similar patterns between the features in both the central and shear margin flow lines. However, features in the margin (combinations of crevasses and channels) are more than twice as rough as features in the central flow line (channels) at similar length scales and experience much higher strain rates. Nonetheless, shear margin features also initiate near the grounding line, deepen rapidly, and then become shallower as they advect to near the calving front. For both the central flow line and shear margin flow line, we speculate that bed geometry around the grounding line may act as an initiation point for features. This hypothesis comes from a qualitative analysis of the initiation of features concerning the underlying bed, in which the bed has a similar shape to the recently formed feature (leftmost feature in Figure 2a and rightmost feature in Figure 4a). This formation is consistent with previous studies (Gladish et al., 2012; Jeofry et al., 2018; O. V. Sergienko, 2013); however, uncertainties in the grounding line location limit us from performing more than a speculative analysis. Likewise, we also observe locations with little obvious signs that bed topography controls the initiation of features. For basal melt channels, subtle effects like sub-glacial discharge (Dallaston et al., 2015; Gladish et al., 2012) or unresolved bed topography (O. V. Sergienko, 2013) could trigger the instability, and these effects suggest that large variations in bed geometry are not necessary for channel initiation but can influence where a channel may form.

4.2. Comparison of Feature Depth Versus Feature Width Across the Pine Island Ice Shelf

The features we analyzed here represent a small fraction of the ice shelf and only a limited portion of the spectrum of features quantified by Watkins et al. (2021). Here we extend the analysis of roughness across the entire ice shelf. Figure 6 shows the depths and widths of all features measured across the Pine Island Ice Shelf, sampled at

500 m resolution. We found that the scaling (power law) from Watkins et al. (2021) continues to hold, with a measured scaling parameter statistically the same in both this study and in Watkins et al. (2021). This relationship also holds for both transverse and longitudinal features taken individually, also consistent with Watkins et al. (2021). In addition, we see that there is a continuous distribution of features without clear clustering along the entire spectrum.

This scaling is intriguing because it supports the hypothesis that melt channels and crevasses exist on a continuum and overlap on the spectrum of features. Because some melt channels may fracture and become large crevasses, and some crevasses may melt and become small melt channels, both sets of features cannot be easily (or statistically) separated into distinct populations. This indicates that, although the features we identified can be roughly classified as "channels" and "crevasses," there are many more features across the ice shelf that have depth/width combinations that fall between these two end members (represented by the clustering of black and red points at each side of Figure 6). We note that error in the BedMachine ice thickness could be propagating into this analysis, causing the spread in the data points analyzed to be somewhat wide. However, the relationship between width and depth for the entire menagerie of features still roughly follows a power-law. Moreover, this result, which suggests that melt channels and crevasses roughly fall on different ends of a scaling spectrum, may potentially help us crudely differentiate between crevasses and channels using (relatively coarse resolution) satellite data.

4.3. High Melt Rates and High Strain Rates Trigger Deeper Channels and Crevasses

To better examine the link between melt channels and crevasses, we analyzed the contribution of strain rate and melt rate to feature roughness. In Figure 5, we observe that features are deepest in all directions when both melt rates and strain rates are high. To further investigate this connection, we explored the relationship between strain rate, melt rate, and roughness for all points on the Pine Island Ice Shelf (Figure 7a). This includes not only the melt channels and shear margins examined in our study but also intermediate features that are not clearly identified as melt channels or crevasses. From Figure 7a, four distinct quadrants emerge. In the bottom left quadrant, where both melt rate and strain rate are low, roughness is minimal ($\leq$5 m). When only the melt rate is high (top left quadrant) or when only the strain rate is high (bottom right quadrant), the roughness is moderate (between 5 and 20 m). Finally, the highest roughness occurs when both strain rate and melt rate are high (top right quadrant of Figure 7a).

For the Pine Island Ice Shelf, the strain rate threshold where we observe a significant increase in roughness occurs at approximately ~0.001 1/day. This aligns with an approximate range of both in situ and remotely sensed values of strain rate required for crevasse initiation (Scott et al., 2010; Wearing et al., 2015). This strain rate corresponds to a deviatoric stress (at −10°C) of around 200 kPa (Wearing et al., 2015), which is similar to the yield strength inferred by Vaughan (1993), although this result may vary among different ice shelves. Additionally, the length scale of these in situ-detected crevasses is much smaller than what we can observe. However, this metric serves as a measure for the initial small-scale crevasse formation. Despite initial brittle crevasses being on the order of tens of millimeters, they can grow rapidly by several meters per year after initiation (Scott et al., 2010). Moreover, the critical strain rate for crevasse propagation is comparable to the critical strain rate where we observe increases in roughness. Overall, these results suggest that large roughness is closely related to both crevassing and melting (greater than 5 m/yr) of ice.

To validate our hypothesis that roughness is highest when both melt rate and strain rate are substantial, we expanded our analysis by incorporating first principal strain rate data from Alley et al. (2018) and melt rate data from Adusumilli et al. (2020) across all Antarctic ice shelves where sufficient data were available. We then conducted the same analysis as performed on the Pine Island Ice Shelf, which is shown in Figure 7b. The results exhibit a similar trend to Figure 7a, suggesting that the findings of this study are applicable to all ice shelves and not exclusive to Pine Island. Furthermore, we have included a series of supplemental figures to reinforce this discussion. First, Figure S4 in Supporting Information S1 illustrates the distribution of roughness values across both Pine Island and all of Antarctica, showcasing the lows and highs of roughness. Second, Figure S5 in Supporting Information S1 depicts the number of measurements in each bin corresponding to Figure 7. Finally, in Figure S6 of the Supporting Information S1, we present the same result as Figure 7, but with a requirement of at least 50 measurements in each bin. Although the resolution of the results in this figure is lower, it demonstrates the same general trend across all ice shelves, indicating that our findings are not sensitive to binning.

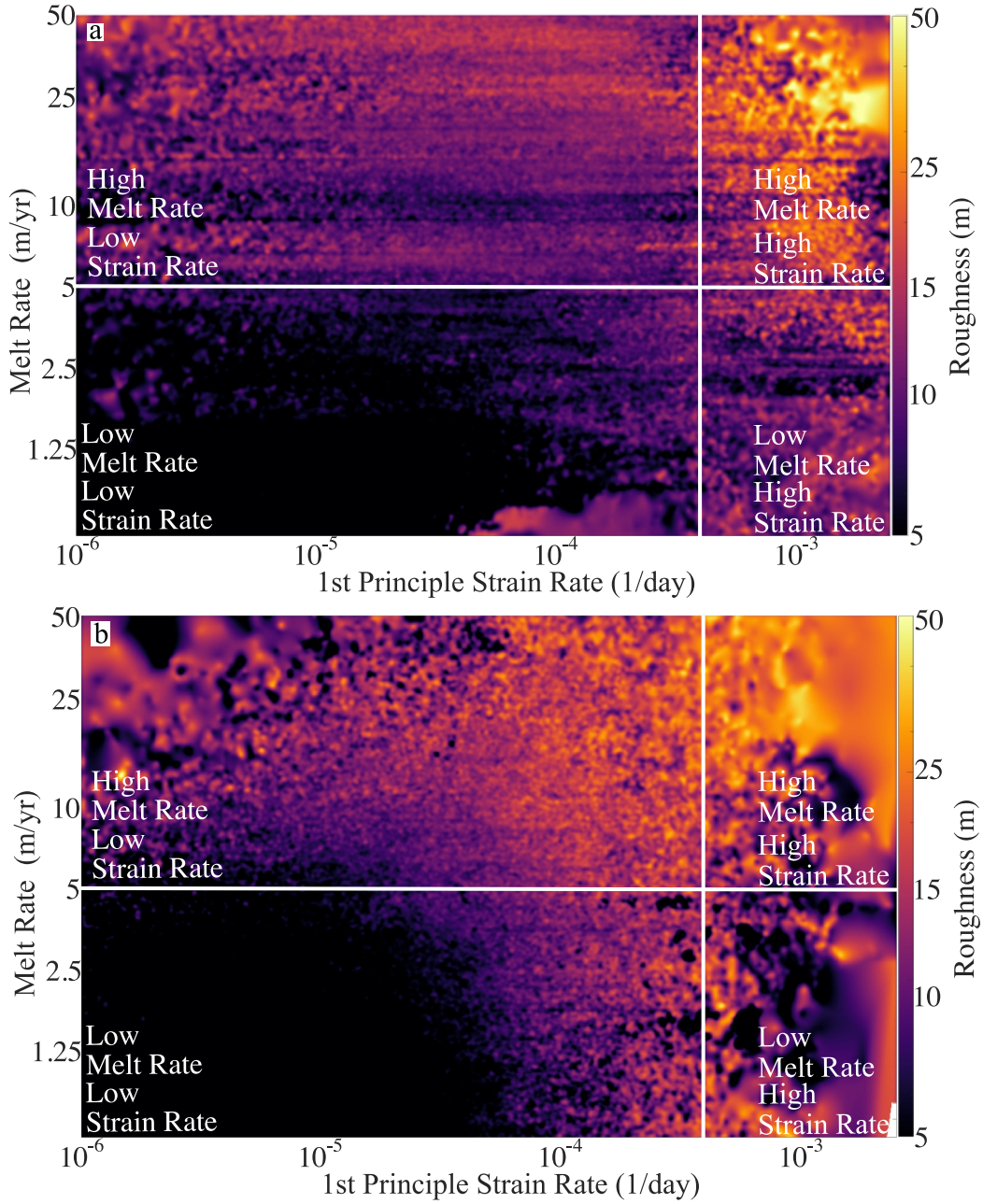

Figure 7. (a) The relationship between the 1st principal strain rate, melt rate, and roughness for the Pine Island Ice Shelf. This figure was generated by compiling all melt rate, strain rate, and roughness data across Pine Island. Using this scatter data, a nearest neighbor interpolation was applied to strain rate and melt rate grids to produce gridded roughness as a function of strain rate and melt rate. Note that other interpolation methods were tested, including plotting the scatter data itself, and the trend remained consistent in each case. Results cluster into four distinct quadrants, with only the upper right quadrant, characterized by high melt rates and high strain rates, resulting in high roughness. (b) The relationship between the 1st principal strain rate, melt rate, and roughness for all Antarctic ice shelves, utilizing strain rates obtained from Alley et al. (2018). Bin sizes in each figure are 0.01 × 0.01 on a logarithmic scale, plotted in linear units.

The observed increase in roughness could stem from a combination of augmented feature depth and width, as documented in Pine Island, or an elevated number of features (e.g., the formation of a closely spaced crevasse field). Previous work (Watkins et al., 2021) suggests that the spectrum of roughness follows a power-law, implying that the processes governing roughness lead to an augmentation in the number of features and increased

depth of existing features. Additionally, some ice shelves examined here are not as densely sampled as Pine Island in the BedMachine model, which could result in additional errors that result in discrepancies between Figures 7a and 7b. However, despite the unclear understanding of the mechanisms responsible for creating roughness on ice shelves and potential errors in BedMachine ice thickness, Figure 7 demonstrates that the rise in roughness associated with melt and strain rate, as determined for Pine Island, extends across a significant portion of ice shelves.

Based on the results of Figure 7, we speculate that the formation and propagation of features (crevasses and melt channels) on ice shelves may be correlated with and largely controlled by processes such as melt and fracture. Melting carves basal melt channels into the base of ice shelves, especially where ice thickness is large and warm ocean waters can intrude and promote channelized melt (Gourmelen et al., 2017). Similarly, where strain rates are high, the ice will fracture, causing crevasses (and potentially rifts) to form. Melt and fracture may also work in combination, where high melt rates increase the stress (Vaughan et al., 2012), resulting in crevasses, and/or basal melt erodes existing crevasses (Washam et al., 2023). The combined effect of these processes could increase roughness and potentially decrease ice stability. Given the current data, we cannot distinguish mechanisms at a high process level. Alternatively, it is possible that high roughness drives increased melt rates and strain rates. However, in the absence of positive feedback that allows melt and strain rate to increase or at least maintain roughness, the increased melt and strain rate would act to diminish roughness over time, contrary to observations of sustained larger increased roughness in high melt regions (Watkins et al., 2021). Moreover, if pre-existing roughness is triggering the increased melt and strain rate, it remains unclear what triggers the initial roughness to begin with. The interpretation that we find more likely is that high strain and high basal melt rates appear to conspire to increase roughness in a mechanism that enhances or maintains roughness over time.

Building on this speculation, it is plausible that pre-existing roughness contributes to increased strain rates and elevated basal melt rates. Theoretical considerations suggest that unless the ice shelf experiences a critically large strain rate (or stress), viscous flow will cause roughness to decay over time (Bassis & Ma, 2015). Similarly, while roughness could augment bottom drag and thereby increase basal melt rates, in the absence of feedbacks where basal melt sustains or increases roughness, this process would eventually erode roughness away.

4.4. Mechanisms for Feature Formation on Ice Shelves and Implications for Ice Shelf Dynamics

Based on the connection between high roughness and the combination of high strain rates and melt rates, we illustrate potential ice shelf feature formation and decay. We hypothesize that high melt rates serve as the seeds for melt channel formation near the grounding line (Figure 8a-a′). However, in regions where strain rates (and stresses) are also sufficiently large to induce ice fracture, these melt channels may also initiate basal crevasses and fracturing events (Figure 8b-b′). This effect has been previously documented in the literature. For instance, Vaughan et al. (2012) demonstrated that the presence of basal channels could trigger basal and surface crevasses. This effect would be amplified for a larger tensile stress field because flexure is a relatively small effect. This mechanism aligns with the proposal by Bindschadler et al. (2011), where they speculate that warm water (in the form of basal melting) can form channels that trigger basal crevasses, or basal crevasses form and are exacerbated by warm water to create channels. Alternatively, in regions where the melt rate is sufficiently high, basal crevasses that form near the grounding line could be more easily excavated by high melt, deepening as they advect.

Either way, the combination of high melt rates and high strain rates results in increased quantity and deeper penetrating melt channels and crevasses on ice shelves. Similarly, portions of channels/crevasses that are not being eroded by basal melting can also trigger basal crevasses (Scott et al., 2010), assuming strain rates are sufficiently high (Figure 8c-c′). However, in the absence of both high melt rates and high strain rates, deformation of the ice will cause topographic features to relax (Bassis & Ma, 2015) (Figure 8d-d′). Alternatively, crevasses (and melt channels that have crevasses within (Vaughan et al., 2012)) can then propagate and turn into full-thickness rifts, which eventually propagate across the ice shelf to isolate an iceberg, thereby triggering a calving event. Increased rifting can result in decreased mechanical integrity and increased potential for ice shelf disintegration (Dow et al., 2018; Liu et al., 2015). This hints that increased melting may be tied to increased ice shelf fracture through the promotion of melt-enhanced rifting, similar to the mechanism proposed in Alley et al. (2019). However, much work remains in identifying the potential links between the penetration depth of deep features on ice shelves and increased rifting, increased calving, and potential ice shelf disintegration.

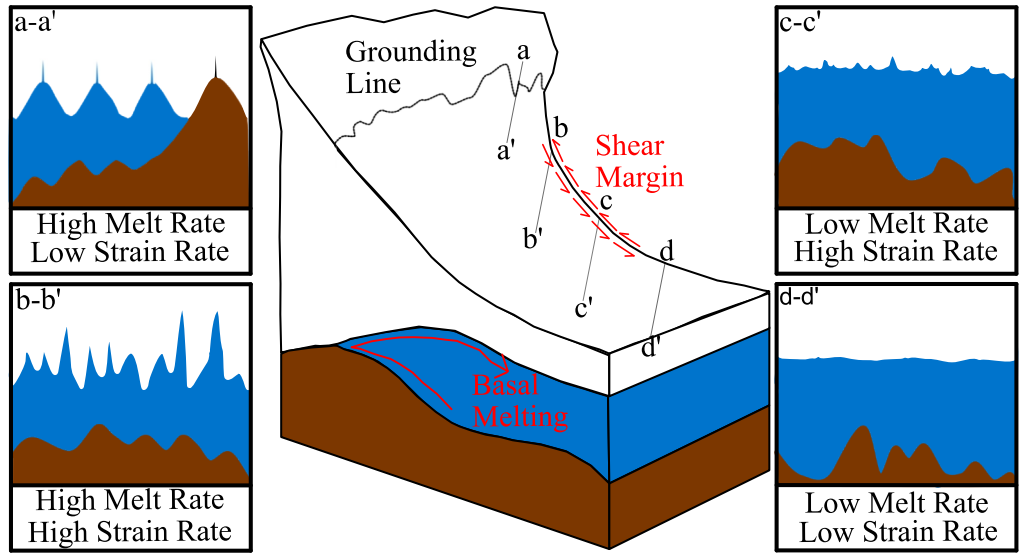

Figure 8. An illustration of the roughening (then smoothing) of an ice shelf. Each of the gray lines represents a transect of the ice taken at an angle to the flow direction. (a) High basal melt rates near the grounding line roughen ice shelves by carving channels. (b) These channels then fracture in high strain rate environments, such as shear margins. (c) As the melt rate decreases toward the middle of the ice shelf and the ice thins, channels disappear. (d) Finally, when strain rates are no longer high, the ice exhibits low roughness at horizontal scales greater than 500 m.

5. Conclusions

Our results build on previous studies that highlight the link between ocean forcing and ice shelf fracture. Consistent with prior research, we find that high melt rates promote basal melt channels with large depths and widths. Additionally, we observed that features in the shear margin have similar characteristics to those in the central flow line, albeit deeper. This results in a roughness that is nearly a factor of two larger. In fact, we find that the roughest sections correspond to the combination of high melt rate and high strain rate on the Pine Island Ice Shelf, where features such as melt channels and crevasses penetrate the deepest in all directions. This result also holds when applied to all Antarctic ice shelves, emphasizing the robustness of this survey. We hypothesize that basal melt and strain rate together contribute to deeper penetrating features on ice shelves. We speculate that these rough features may, in turn, promote increased fracturing of ice, however, our analysis cannot fully distinguish between mechanisms that cause roughness. It is possible that there are feedbacks where increased roughness results in increased basal melt and vice versa. These processes need better understanding to assess their importance to ice shelf mechanics. Additionally, further work remains in directly tying roughness—shown here to be a proxy for the presence of basal melt channels and crevasses—to increased calving, melt, and retreat of ice shelves.

Our comprehension of ice shelf roughness and its potential diagnostic significance is still in its early stages. Recent studies continue to emphasize the intricate interplay between basal melt and crevasses (Alley et al., 2021; Washam et al., 2023). Similarly, Larter (2022) recently suggested that roughness may serve as a health indicator for ice shelves. The causes and consequences of roughness on the dynamics of ice shelves need more thorough exploration, both at the process level and by examining the evolution of roughness across ice shelves (i.e., a time series of roughness). This approach may prove useful in diagnosing which ice shelves may be susceptible to future increases in melt and fracture.

Data Availability Statement

The BedMachine Antarctica data is accessible at https://nsidc.org/data/nsidc-0756/versions/2. Melt Rate data is available at http://library.ucsd.edu/dc/object/bb0448974g. Pine Island strain rate data can be obtained by

contacting the authors upon request. Antarctic strain rate data is available through Alley et al. (2018). Ice velocity data, utilized in calculating flowlines, is accessible at https://nsidc.org/data/nsidc-0484/versions/2.

Acknowledgments
This work is funded by NASA Grant 80NSSC22K0378 and is also partially supported by the DOMINOS project, a component of the International Thwaites Glacier Collaboration (ITGC). Additional support comes from the National Science Foundation (NSF: Grant 1738896) and the Natural Environment Research Council (NERC: Grant NE/S006605/1). Logistics were provided by NSF-U.S. Antarctic Program and NERC-British Antarctic Survey. Mapping was conducted with the assistance of the Antarctic Mapping Toolbox in MATLAB (Greene et al., 2017). We would like to also thank our three reviewers as well as the associate editor and editor for their insightful feedback in reviewing this manuscript.

References

Adusumilli, S., Fricker, H. A., Medley, B., Padman, L., & Siegfried, M. R. (2020). Interannual variations in meltwater input to the Southern Ocean from Antarctic ice shelves. *Nature Geoscience*, *13*(9), 616–620. https://doi.org/10.1038/s41561-020-0616-z

Alley, K. E., Scambos, T. A., & Alley, R. B. (2023). The role of channelized basal melt in ice-shelf stability: Recent progress and future priorities. *Annals of Glaciology*, *63*(87–89), 1–5. https://doi.org/10.1017/aog.2023.5

Alley, K. E., Scambos, T. A., Alley, R. B., & Holschuh, N. (2019). Troughs developed in ice-stream shear margins precondition ice shelves for ocean-driven breakup. *Science Advances*, *5*(10). https://doi.org/10.1126/sciadv.aax2215

Alley, K. E., Scambos, T. A., Anderson, R. S., Rajaram, H., Pope, A., & Haran, T. M. (2018). Continent-wide estimates of Antarctic strain rates from Landsat 8-derived velocity grids. *Journal of Glaciology*, *64*(244), 321–332. https://doi.org/10.1017/jog.2018.23

Alley, K. E., Scambos, T. A., Siegfried, M. R., & Fricker, H. A. (2016). Impacts of warm water on Antarctic ice shelf stability through basal channel formation. *Nature Geoscience*, *9*(4), 290–293. https://doi.org/10.1038/ngeo2675

Alley, K. E., Wild, C. T., Luckman, A., Scambos, T. A., Truffer, M., Pettit, E. C., et al. (2021). Two decades of dynamic change and progressive destabilization on the Thwaites Eastern Ice Shelf. *The Cryosphere*, *15*(11), 5187–5203. https://doi.org/10.5194/tc-15-5187-2021

Arndt, J. E., Larter, R. D., Friedl, P., Gohl, K., & and, K. H. (2018). Bathymetric controls on calving processes at Pine Island Glacier. *The Cryosphere*, *12*(6), 2039–2050. https://doi.org/10.5194/tc-12-2039-2018

Banwell, A. F., MacAyeal, D. R., & Sergienko, O. V. (2013). Breakup of the Larsen B Ice Shelf triggered by chain reaction drainage of supraglacial lakes. *Geophysical Research Letters*, *40*(22), 5872–5876. https://doi.org/10.1002/2013gl057694

Bassis, J. N., & Jacobs, S. (2013). Diverse calving patterns linked to glacier geometry. *Nature Geoscience*, *6*(10), 833–836. https://doi.org/10.1038/ngeo1887

Bassis, J. N., & Ma, Y. (2015). Evolution of basal crevasses links ice shelf stability to ocean forcing. *Earth and Planetary Science Letters*, *409*, 203–211. https://doi.org/10.1016/j.epsl.2014.11.003

Bassis, J. N., & Walker, C. C. (2011). Upper and lower limits on the stability of calving glaciers from the yield strength envelope of ice. *Proceedings of the Royal Society A: Mathematical, Physical and Engineering Sciences*, *468*(2140), 913–931. https://doi.org/10.1098/rspa.2011.0422

Bindschadler, R., Vaughan, D. G., & Vornberger, P. (2011). Variability of basal melt beneath the Pine Island Glacier ice shelf, West Antarctica. *Journal of Glaciology*, *57*(204), 581–595. https://doi.org/10.3189/002214311797409802

Bishop, M. P., Björnsson, H., Haeberli, W., Oerlemans, J., Shroder, J. F., & Tranter, M. (2011). *Encyclopedia of snow, ice and glaciers*. Springer Science & Business Media.

Dallaston, M. C., Hewitt, I. J., & Wells, A. J. (2015). Channelization of plumes beneath ice shelves. *Journal of Fluid Mechanics*, *785*, 109–134. https://doi.org/10.1017/jfm.2015.609

Doake, C. S. M., Corr, H. F. J., Rott, H., Skvarca, P., & Young, N. W. (1998). Breakup and conditions for stability of the northern Larsen Ice Shelf, Antarctica. *Nature*, *391*(6669), 778–780. https://doi.org/10.1038/35832

Dow, C. F., Lee, W. S., Greenbaum, J. S., Greene, C. A., Blankenship, D. D., Poinar, K., et al. (2018). Basal channels drive active surface hydrology and transverse ice shelf fracture. *Science Advances*, *4*(6). https://doi.org/10.1126/sciadv.aao7212

Drews, R. (2015). Evolution of ice-shelf channels in Antarctic ice shelves. *The Cryosphere*, *9*(3), 1169–1181. https://doi.org/10.5194/tc-9-1169-2015

Dupont, T. K., & Alley, R. B. (2005). Assessment of the importance of ice-shelf buttressing to ice-sheet flow. *Geophysical Research Letters*, *32*(4), L04503. https://doi.org/10.1029/2004gl022024

Dutrieux, P., Vaughan, D. G., Corr, H. F. J., Jenkins, A., Holland, P. R., Joughin, I., & Fleming, A. H. (2013). Pine Island glacier ice shelf melt distributed at kilometre scales. *The Cryosphere*, *7*(5), 1543–1555. https://doi.org/10.5194/tc-7-1543-2013

Favier, L., Pattyn, F., Berger, S., & Drews, R. (2016). Dynamic influence of pinning points on marine ice-sheet stability: A numerical study in Dronning Maud Land, East Antarctica. *The Cryosphere*, *10*(6), 2623–2635. https://doi.org/10.5194/tc-10-2623-2016

Fürst, J. J., Durand, G., Gillet-Chaulet, F., Tavard, L., Rankl, M., Braun, M., & Gagliardini, O. (2016). The safety band of Antarctic ice shelves. *Nature Climate Change*, *6*(5), 479–482. https://doi.org/10.1038/nclimate2912

Gladish, C. V., Holland, D. M., Holland, P. R., & Price, S. F. (2012). Ice-shelf basal channels in a coupled ice/ocean model. *Journal of Glaciology*, *58*(212), 1227–1244. https://doi.org/10.3189/2012jog12j003

Gourmelen, N., Goldberg, D. N., Snow, K., Henley, S. F., Bingham, R. G., Kimura, S., et al. (2017). Channelized melting drives thinning under a rapidly melting Antarctic ice shelf. *Geophysical Research Letters*, *44*(19), 9796–9804. https://doi.org/10.1002/2017gl074929

Greene, C. A., Gardner, A. S., Schlegel, N.-J., & Fraser, A. D. (2022). Antarctic calving loss rivals ice-shelf thinning. *Nature*, *609*(7929), 948–953. https://doi.org/10.1038/s41586-022-05037-w

Greene, C. A., Gwyther, D. E., & Blankenship, D. D. (2017). Antarctic mapping tools for MATLAB. *Computers & Geosciences*, *104*, 151–157. https://doi.org/10.1016/j.cageo.2016.08.003

Gudmundsson, G. H. (2013). Ice-shelf buttressing and the stability of marine ice sheets. *The Cryosphere*, *7*(2), 647–655. https://doi.org/10.5194/tc-7-647-2013

Haseloff, M., & Sergienko, O. (2018). The effect of buttressing on grounding line dynamics. *Journal of Glaciology*, *64*(245), 417–431. https://doi.org/10.1017/jog.2018.30

Humbert, A., Christmann, J., Corr, H. F. J., Helm, V., Höyns, L.-S., Hofstede, C., et al. (2022). On the evolution of an ice shelf melt channel at the base of Filchner Ice Shelf, from observations and viscoelastic modeling. *The Cryosphere*, *16*(10), 4107–4139. https://doi.org/10.5194/tc-16-4107-2022

Ishalina, O. T., Bliakharskii, D. P., & Florinsky, I. V. (2021). Recognition of crevasses with high-resolution digital elevation models: Application of geomorphometric modeling and texture analysis. *Transactions in GIS*, *25*(5), 2529–2552. https://doi.org/10.1111/tgis.12790

Jenkins, A., Shoosmith, D., Dutrieux, P., Jacobs, S., Kim, T. W., Lee, S. H., et al. (2018). West Antarctic Ice Sheet retreat in the Amundsen Sea driven by decadal oceanic variability. *Nature Geoscience*, *11*(10), 733–738. https://doi.org/10.1038/s41561-018-0207-4

Jeofry, H., Ross, N., Brocq, A. L., Graham, A. G., Li, J., Gogineni, P., et al. (2018). Hard rock landforms generate 130 km ice shelf channels through water focusing in basal corrugations. *Nature Communications*, *9*(1), 4576. https://doi.org/10.1038/s41467-018-06679-z

Jeong, S., Howat, I. M., & Bassis, J. N. (2016). Accelerated ice shelf rifting and retreat at Pine Island Glacier, West Antarctica. *Geophysical Research Letters*, *43*(22), 11720–11725. https://doi.org/10.1002/2016gl071360

Joughin, I., Shapero, D., Smith, B., Dutrieux, P., & Barham, M. (2021). Ice-shelf retreat drives recent Pine Island Glacier speedup. *Science Advances*, *7*(24), eabg3080. https://doi.org/10.1126/sciadv.abg3080

Kulessa, B., Jansen, D., Luckman, A. J., King, E. C., & Sammonds, P. R. (2014). Marine ice regulates the future stability of a large Antarctic ice shelf. *Nature Communications*, *5*(1), 3707. https://doi.org/10.1038/ncomms4707

Lai, C.-Y., Kingslake, J., Wearing, M. G., Chen, P.-H. C., Gentine, P., Li, H., et al. (2020). Vulnerability of Antarctica's ice shelves to meltwater-driven fracture. *Nature*, *584*(7822), 574–578. https://doi.org/10.1038/s41586-020-2627-8

Larour, E., Rignot, E., Poinelli, M., & Scheuchl, B. (2021). Physical processes controlling the rifting of Larsen C Ice Shelf, Antarctica, prior to the calving of iceberg A68. *Proceedings of the National Academy of Sciences of the United States of America*, *118*(40). https://doi.org/10.1073/pnas.2105080118

Larter, R. D. (2022). Basal melting, roughness and structural integrity of ice shelves. *Geophysical Research Letters*, *49*(4), e2021GL097421. https://doi.org/10.1029/2021gl097421

Lhermitte, S., Sun, S., Shuman, C., Wouters, B., Pattyn, F., Wuite, J., et al. (2020). Damage accelerates ice shelf instability and mass loss in Amundsen Sea embayment. *Proceedings of the National Academy of Sciences of the United States of America*, *117*(40), 24735–24741. https://doi.org/10.1073/pnas.1912890117

Liu, Y., Moore, J. C., Cheng, X., Gladstone, R. M., Bassis, J. N., Liu, H., et al. (2015). Ocean-driven thinning enhances iceberg calving and retreat of Antarctic ice shelves. *Proceedings of the National Academy of Sciences of the United States of America*, *112*(11), 3263–3268. https://doi.org/10.1073/pnas.1415137112

Luckman, A., Benn, D. I., Cottier, F., Bevan, S., Nilsen, F., & Inall, M. (2015). Calving rates at tidewater glaciers vary strongly with ocean temperature. *Nature Communications*, *6*(1), 8566. https://doi.org/10.1038/ncomms9566

Marsh, O. J., Fricker, H. A., Siegfried, M. R., Christianson, K., Nicholls, K. W., Corr, H. F. J., & Catania, G. (2016). High basal melting forming a channel at the grounding line of Ross Ice Shelf, Antarctica. *Geophysical Research Letters*, *43*(1), 250–255. https://doi.org/10.1002/2015gl066612

McGrath, D., Steffen, K., Scambos, T. A., Rajaram, H., Casassa, G., & Lagos, J. L. R. (2012). Basal crevasses and associated surface crevassing on the Larsen C Ice Shelf, Antarctica, and their role in ice-shelf instability. *Annals of Glaciology*, *53*(60), 10–18. https://doi.org/10.3189/2012aog60a005

Morlighem, M. (2019). *Measures bedmachine Antarctica, version 1*. NASA National Snow and Ice Data Center DAAC. https://doi.org/10.5067/c2gfer6ptos4

Morlighem, M., Rignot, E., Binder, T., Blankenship, D., Drews, R., Eagles, G., et al. (2019). Deep glacial troughs and stabilizing ridges unveiled beneath the margins of the Antarctic ice sheet. *Nature Geoscience*, *13*(2), 132–137. https://doi.org/10.1038/s41561-019-0510-8

Nakayama, Y., Manucharyan, G., Zhang, H., Dutrieux, P., Torres, H. S., Klein, P., et al. (2019). Pathways of ocean heat towards Pine Island and Thwaites grounding lines. *Scientific Reports*, *9*(1), 16649. https://doi.org/10.1038/s41598-019-53190-6

Obase, T., Abe-Ouchi, A., Kusahara, K., Hasumi, H., & Ohgaito, R. (2017). Responses of basal melting of Antarctic ice shelves to the climatic forcing of the Last Glacial Maximum and CO_2 doubling. *Journal of Climate*, *30*(10), 3473–3497. https://doi.org/10.1175/jcli-d-15-0908.1

Paden, J., Li, J., Leuschen, C., Rodriguez-Morales, F., & Hale, R. (2010). *IceBridge MCoRDS l2 ice thickness, version 1*. NASA National Snow and Ice Data Center Distributed Active Archive Center. https://doi.org/10.5067/gdq0cucvte2q

Rignot, E., Casassa, G., Gogineni, P., Krabill, W., Rivera, A., & Thomas, R. (2004). Accelerated ice discharge from the Antarctic Peninsula following the collapse of Larsen B ice shelf. *Geophysical Research Letters*, *31*(18), L18401. https://doi.org/10.1029/2004gl020697

Rignot, E., Jacobs, S., Mouginot, J., & Scheuchl, B. (2013). Ice-shelf melting around Antarctica. *Science*, *341*(6143), 266–270. https://doi.org/10.1126/science.1235798

Rignot, E., Mouginot, J., Morlighem, M., Seroussi, H., & Scheuchl, B. (2014). Widespread, rapid grounding line retreat of Pine Island, Thwaites, Smith, and Kohler glaciers, West Antarctica, from 1992 to 2011. *Geophysical Research Letters*, *41*(10), 3502–3509. https://doi.org/10.1002/2014gl060140

Rignot, E., Mouginot, J., Scheuchl, B., van den Broeke, M., van Wessem, M. J., & Morlighem, M. (2019). Four decades of Antarctic Ice Sheet mass balance from 1979–2017. *Proceedings of the National Academy of Sciences of the United States of America*, *116*(4), 1095–1103. https://doi.org/10.1073/pnas.1812883116

Robel, A. A., & Banwell, A. F. (2019). A speed limit on ice shelf collapse through hydrofracture. *Geophysical Research Letters*, *46*(21), 12092–12100. https://doi.org/10.1029/2019gl084397

Scambos, T. A., Bohlander, J. A., Shuman, C. A., & Skvarca, P. (2004). Glacier acceleration and thinning after ice shelf collapse in the Larsen B embayment, Antarctica. *Geophysical Research Letters*, *31*(18), L18402. https://doi.org/10.1029/2004gl020670

Scambos, T. A., Hulbe, C., & Fahnestock, M. (2003). Climate-induced ice shelf disintegration in the Antarctic Peninsula. In *Antarctic Peninsula climate variability: Historical and paleoenvironmental perspectives* (pp. 79–92). American Geophysical Union. https://doi.org/10.1029/ar079p0079

Schmidt, B. E., Washam, P., Davis, P. E. D., Nicholls, K. W., Holland, D. M., Lawrence, J. D., et al. (2023). Heterogeneous melting near the Thwaites Glacier grounding line. *Nature*, *614*(7948), 471–478. https://doi.org/10.1038/s41586-022-05691-0

Scott, J. B., Smith, A. M., Bingham, R. G., & Vaughan, D. G. (2010). Crevasses triggered on Pine Island Glacier, West Antarctica, by drilling through an exceptional melt layer. *Annals of Glaciology*, *51*(55), 65–70. https://doi.org/10.3189/172756410791392763

Sergienko, O., & Haseloff, M. (2023). 'Stable' and 'unstable' are not useful descriptions of marine ice sheets in the Earth's climate system. *Journal of Glaciology*, *69*(277), 1483–1499. https://doi.org/10.1017/jog.2023.40

Sergienko, O. V. (2013). Basal channels on ice shelves. *Journal of Geophysical Research: Earth Surface*, *118*(3), 1342–1355. https://doi.org/10.1002/jgrf.20105

Shean, D. E., Joughin, I. R., Dutrieux, P., Smith, B. E., & Berthier, E. (2019). Ice shelf basal melt rates from a high-resolution digital elevation model (DEM) record for Pine Island Glacier, Antarctica. *The Cryosphere*, *13*(10), 2633–2656. https://doi.org/10.5194/tc-13-2633-2019

Sifuzzaman, M. (2009). Application of wavelet transform and its advantages compared to Fourier transform.

Still, H., Campbell, A., & Hulbe, C. (2018). Mechanical analysis of pinning points in the Ross Ice Shelf, Antarctica. *Annals of Glaciology*, *60*(78), 32–41. https://doi.org/10.1017/aog.2018.31

Stoica, P., & Moses, R. L. (2005). *Spectral analysis of signals*. Pearson.

Surawy-Stepney, T., Hogg, A. E., Cornford, S. L., & Davison, B. J. (2023). Episodic dynamic change linked to damage on the Thwaites Glacier Ice Tongue. *Nature Geoscience*, *16*(1), 37–43. https://doi.org/10.1038/s41561-022-01097-9

Vaughan, D. G. (1993). Relating the occurrence of crevasses to surface strain rates. *Journal of Glaciology*, *39*(132), 255–266. https://doi.org/10.3189/s0022143000015926

Vaughan, D. G., Corr, H. F. J., Bindschadler, R. A., Dutrieux, P., Gudmundsson, G. H., Jenkins, A., et al. (2012). Subglacial melt channels and fracture in the floating part of Pine Island Glacier, Antarctica. *Journal of Geophysical Research*, *117*(F3), F03012. https://doi.org/10.1029/2012jf002360

Wåhlin, A. K., Graham, A. G. C., Hogan, K. A., Queste, B. Y., Boehme, L., Larter, R. D., et al. (2021). Pathways and modification of warm water flowing beneath Thwaites Ice Shelf, West Antarctica. *Science Advances*, *7*(15). https://doi.org/10.1126/sciadv.abd7254

Washam, P., Lawrence, J. D., Stevens, C. L., Hulbe, C. L., Horgan, H. J., Robinson, N. J., et al. (2023). Direct observations of melting, freezing, and ocean circulation in an ice shelf basal crevasse. *Science Advances*, *9*(43). https://doi.org/10.1126/sciadv.adi7638

Watkins, R. H., Bassis, J. N., & Thouless, M. D. (2021). Roughness of ice shelves is correlated with basal melt rates. *Geophysical Research Letters*, *48*(21), e2021GL094743. https://doi.org/10.1029/2021gl094743

Wearing, M. G., Hindmarsh, R. C., & Worster, M. G. (2015). Assessment of ice flow dynamics in the zone close to the calving front of Antarctic ice shelves. *Journal of Glaciology*, *61*(230), 1194–1206. https://doi.org/10.3189/2015jog15j116

Whitehouse, D. J. (2004). *Surfaces and their measurement*. Kogan Page Science.

Wild, C. T., Alley, K. E., Muto, A., Truffer, M., Scambos, T. A., & Pettit, E. C. (2022). Weakening of the pinning point buttressing Thwaites Glacier, West Antarctica. *The Cryosphere*, *16*(2), 397–417. https://doi.org/10.5194/tc-16-397-2022